Fundamental processes in nanosecond pulsed laser ablation of metals in vacuum

P. Écija, M. N. Sánchez Rayo, R. Martínez, B. Sierra, C. Redondo, F. J. Basterretxea, and F. Castaño*
Department of Chemical Physics, University of the Basque Country, Campus of Leioa, Barrio Sarriena s/n, 48940 Leioa, Spain
(Received 27 February 2007; revised manuscript received 24 December 2007; published 17 March 2008)

Velocity and kinetic energy distributions (VDs, KEDs) of metal ions generated by nanosecond (ns) pulsed laser ablation under high vacuum have been determined using an electrostatic analyzer plus time-of-flight coupled system. A number of metal and alloy targets, principally involving Fe and Ni, have been studied at different laser fluences. At low fluence, the ion distributions have been shown to fit single Maxwell-Boltzmann-Coulomb (MBC) distributions; for medium and higher fluences, each ion distribution is found to comprise that of the surviving "precursor" ion, itself, overlapped with sidebands which arise from ion-electron recombination and/or ionization. The so-called surviving "precursor" ion of a distribution is that which underwent no change of charge. The Coulomb velocities of the surviving "precursor" ions and those of the ion products resulting from ion-electron collisions have been compared. Ion velocities are correlated with the local electric field resulting from ejection of the photoelectrons following laser ablation. Under identical conditions of laser fluence, the ions are seen to experience an electrical field nearly independent of their charge. The transit times of ions in the plasma have been estimated to be of the order of 1 ps. An overall quantitative mechanism for metal ablation on this basis is presented, including the ejection time for photoelectrons and differences in ion distributions resulting from employing laser pulses in the nanosecond (ns) and femtosecond (fs) regimes.

DOI: 10.1103/PhysRevA.77.032904 PACS number(s): 79.20.Ds, 34.70.+e, 34.80.−i, 82.30.Fi

I. INTRODUCTION

A large number of studies of laser ablated metals have been reported in recent years on account of technical [1,2], analytical [3–5], and high-energy applications [6]. These include material deposition [pulsed-laser deposition (PLD)], etching, cutting, doping, lithography, soldering, microelectromechanical systems (MEMS) and nanoelectromechanical systems (NEMS) fabrication [1,2], laser-induced breakdown spectroscopy (LIBS) and laser-induced plasma spectroscopy (LIPS) [3–5], and ion beam injection [6]. The detection of optical emission from ions and neutrals following such ablation is routinely employed to identify the composition of complex materials such as minerals, high-temperature superconductors, and alloys.

In fundamental terms, laser ablation is initiated by applying a large electromagnetic field onto a very small area on the material surface thus providing sufficient energy to eject photoelectrons and melt, dissociate, and evaporate the metal. In turn, this yields a plasma with highly excited atomic and ionic states together with electrons, and where the energy excess is finally relaxed as thermal energy and radiation to the neighborhood [7]. Investigation of the mechanism thus requires detailed study of this radiation and the particles that are ejected. The observation of x-ray emission at laser fluences employed in such studies is rare and usually neglected. Visible and ultraviolet emission is subject to radiation trapping by the plasma where, for example, the density of an Fe plasma using fluences of magnitude 1.2–13.1 J cm^{-2} [8,9], would be computed to be in the range (2.7–4.5) $\times 10^{20}$ cm^{-3}, lengthening effective mean radiative lifetimes by several orders of magnitude and which become longer than the ablation processes itself. The energy of the visible or uv radiation emitted from the metal atoms (2–6 eV) is several orders of magnitude smaller than that of other particles and thus provides little information on the mechanism of the ablation process. Later photothermal relaxation into the bulk material is difficult to measure, particularly in real time. Thus the only particles that may be effectively employed to characterize the mechanism of the ablation process are the ejected ions and neutrals. As subsequently shown here, the average kinetic energy of ejected metal ions reach several hundred eV, larger than that for any other observable particles and hence are employed as probes for describing the ablation process.

Since the absorbed laser radiation yields a decrease in the electron density and an increase of the ion density inside the metal, subsequent rapid collisions in the nanosecond regime are postulated (usually neglected and never observed [9]) to yield a range of species according to the standard ionic reactions:

$$A^{n+} + e^- \rightarrow A^{(n-1)+}, \quad \text{recombination process}, \tag{1}$$

$$A^{n+} + e^- \rightarrow A^{(n+1)+} + 2e^-, \quad \text{ionization process}, \tag{2}$$

$$A^{n+} + A^{n'+} \rightarrow A^{n''+} + A^{(n+n'-n'')+}, \quad \text{disproportionation, ion charge interchange}, \tag{3}$$

$$(A^{n+})^{**} \rightarrow (A^{n+})^{*} + h\nu, \quad \text{radiation trapping and/or relaxation to phonons}. \tag{4}$$

Rate constants for these reactions inside the high-density plasma are unknown and, because the environment is one of high electric and magnetic fields and temperature, the overall

*Author to whom correspondence should be addressed: f.castano@ehu.es

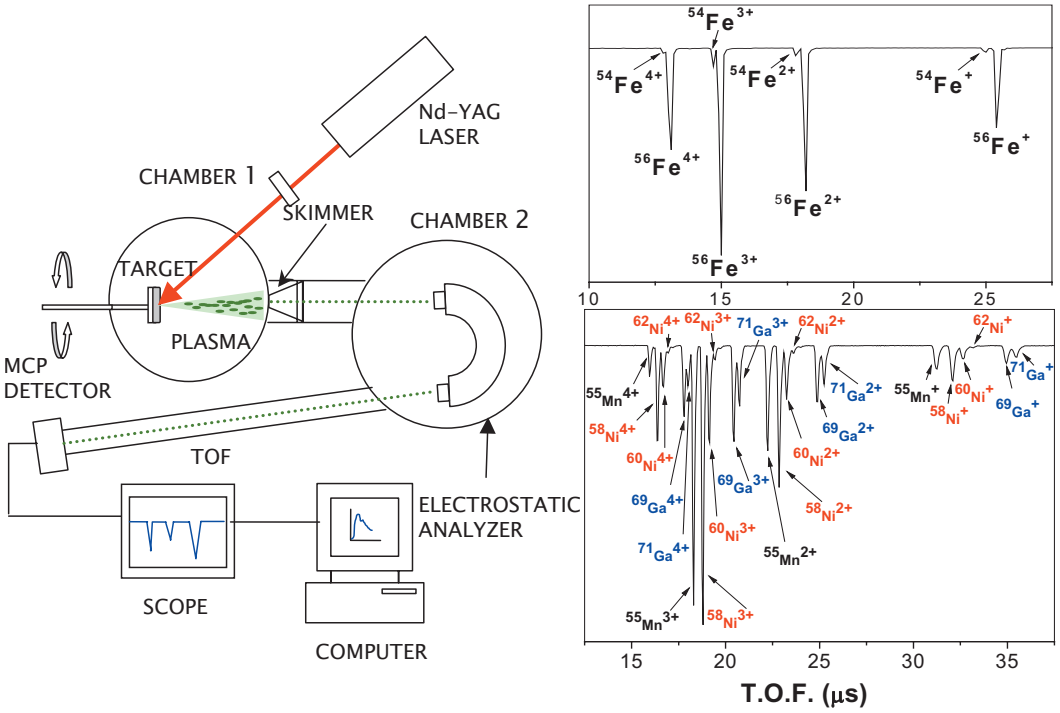

FIG. 1. (Color) Experimental arrangement for measurement of the velocity distribution of ions ejected by laser ablation on metals and alloys. Insets: TOF spectra of Fe ions by laser ablation from an Fe target (fluence 13.1 J cm^{-2}) and Ni, Mn, and Ga ions from a Ni_2MnGa target (fluence 14.7 J cm^{-2}). The electrostatic analyzer was set at ΔV=220.4 V for Fe and 145.6 V for Ni (corresponding to an energy given by $E=2.25\times Z\Delta V$ where Z is the charge of the ion).

rates are expected to be much faster than those normally encountered in the gas phase. Electron-ion energy transfer has been estimated to take place in <1 ps [9], yielding higher charged ions [2] and/or recombined ions [1], so that they are created and ejected at high velocities from the plasma plume.

A limited number of ion distributions following ablation of metals have been reported [10–14] and, in some cases, it has been suggested that these are Maxwell-Boltzmann-Coulomb (MBC) distributions in character [7,8,12]. Experimental velocity distributions, particularly for medium and high laser fluences (2–15 J cm^{-2}), are required to characterize the parameters of such plasmas, in turn used for constructing theoretical distributions which can then be compared with observed distributions in general and account for such phenomena as "sidebands" and their origins. The generation of these sidebands and their role in the ablation model is one of the major objectives of this investigation as it provides a quantitative guide to the overall mechanism incorporating the above reactions.

II. EXPERIMENT

The experimental arrangement for measuring either velocity distributions (VDs) or their equivalent kinetic energy distributions (KEDs) following metal laser ablation is depicted schematically in Fig. 1. Ablation is accomplished with a frequency-doubled 3.7 ns pulsed Nd–yttrium-aluminum-garnet (YAG) laser beam (Quantel, model Brilliant B) operating at 10 Hz repetition rate. The laser beam is focused by a quartz lens (f=500 mm) onto a rotating target placed inside a chamber at a working pressure of 10^{-7} mbar. The laser beam impinges onto the metal at 30° from the normal to the target plane and the resulting ions normal to the target plane are selected through a 1 mm ϕ skimmer further directed to the opening of the electrostatic analyzer (Comstock AC-901). This selects ions by their charge and/or mass ratios by scanning the voltage difference ΔV (corresponding to the energy $E=2.25\times Z\Delta V$, where Z is the ionic charge and 2.25 the geometrical factor of the analyzer) between the analyzer's hemispherical plates. The ions are subsequently directed into the axis of the drift tube of a time-of-flight (TOF) analyzer and finally reach a multichannel plate (MCP) detector. The laser fluence was varied in the range 1–15 J cm^{-2}.

Examples of mass spectra from Fe and Ni_2MnGa targets are shown as insets in Fig. 1. Fe spectra were recorded at 220.4 V (E/Z 496 eV) for a fluence of 9.2 J cm^{-2} whereas those from Ni_2MnGa were recorded at 145.6 V (E/Z 328 eV) for a fluence of 14.7 J cm^{-2}. The band intensity ratios of the Fe, Ni, Mn, and Ga isotopes match faithfully their natural abundances [15] where identical outcome ratios are observed in all other spectra at the fluences reported. The density of any ejected ion selected by the electrostatic analyzer is proportional to the area of its TOF mass spectrum band and thus the plot of these areas as a function of ΔV, or indeed the kinetic energy, provides the required distribution.

III. RESULTS AND DISCUSSION

Figure 2 gives some examples of experimental KEDs for Fe ions from an Fe target at fluences of 6.8 and 13.1 J cm^{-2}

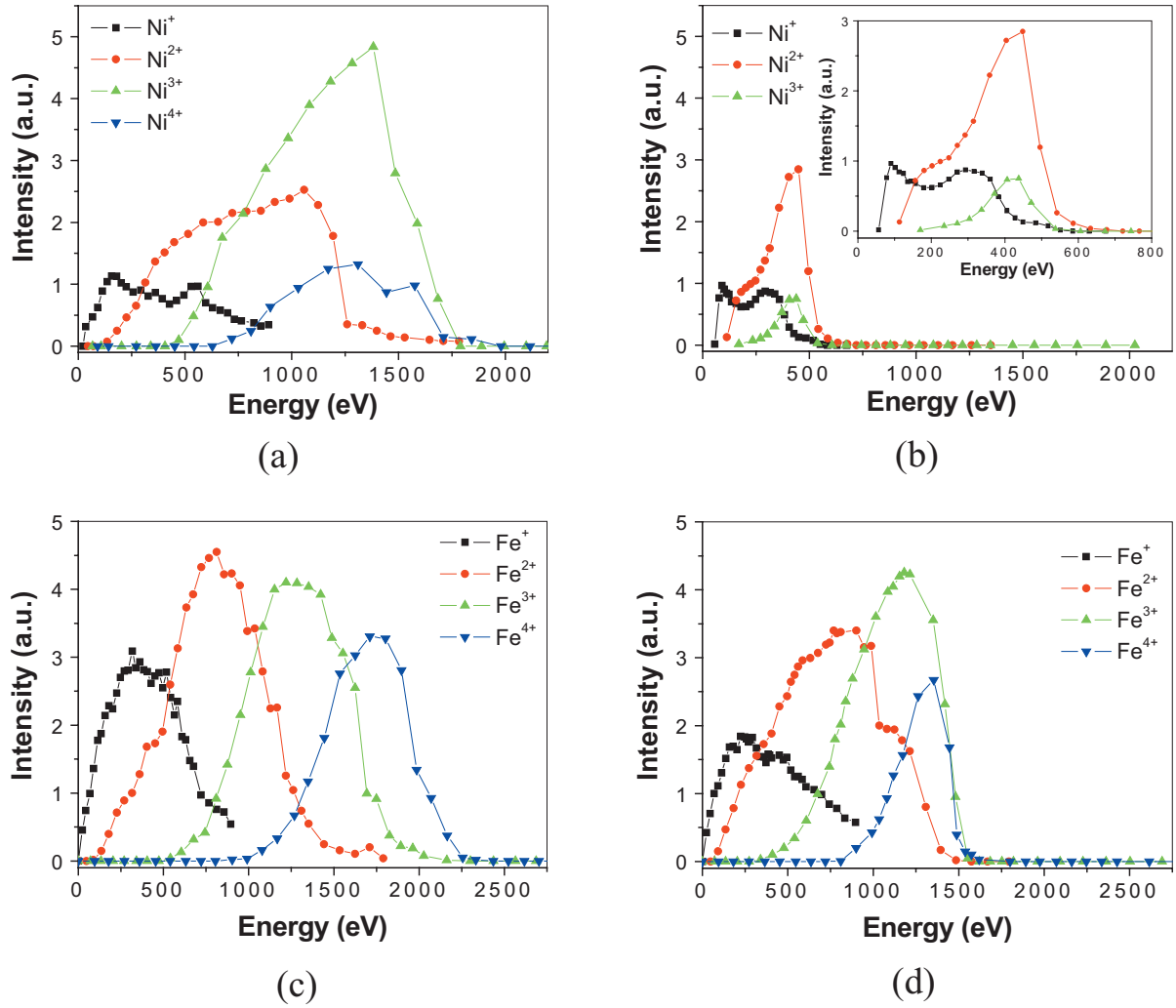

FIG. 2. (Color) Experimental kinetic energy distributions (KEDs) for Ni ions from a Ni_2MnGa target at laser fluences of (a) 14.7 J cm^{-2} and (b) 3.7 J cm^{-2}, and for Fe ions from an Fe target at laser fluences of (c) 13.1 J cm^{-2} and (d) 6.8 J cm^{-2}. The lines joining the experimental points are visual guides.

and Ni ions from a Ni_2MnGa target at fluences of 3.7 and 14.7 J cm^{-2}. The shapes of the distributions are significantly different and do not fit a single MBC distribution or any other single distribution. Distributions for a range of ions such as Fe^{n+} (n=1–4), Ni^{n+} (n=0–4), Mn^{n+} (n=0–4), and Ga^{n+} (n=0–4) have been characterized. For the medium and high fluences employed, the distributions are rather complex, with different shapes for Fe and Ni ions and do not fit any single elementary distribution. This contrasts with the excellent fit to shifted Maxwell-Boltzmann distributions for single ion appearance for Fe^+ and Ni^+, just over threshold fluence, not shown here.

Population ratios for any states i and j of a given ion are taken to be described by Boltzmann distributions, $N_i/N_j = \exp[-(E_i - E_j)/kT]$, where the symbols have their usual meaning. The leading contributions to the total kinetic energy results from the velocity in the propagation direction v_x, the flow velocity for the supersonic expansion v_k [16,17], and the Coulomb velocity in the propagation direction v_c [12]. A plot of the maximum in the experimental energy distribution versus the ion charge yields a quasilinear dependence taken to justify the introduction of a charge related velocity (see below). Using the standard derivation for the kinetic energy and velocity distributions, the following expression is obtained:

$$F(v_x, v_c) = A(m/2\pi kT)^{3/2} v_x^3 \exp[-m(v_x - v_k - v_c)^2/2kT], \tag{5}$$

where A is the distribution normalization constant. For an observed ion at a preset fluence, the velocities v_x and v_k are fixed. However, the Coulomb velocity, v_c, which is proportional to the charge of the ion [12], is unique only if the observed ions do not undergo any changes. In ablation, the densities of ions, electrons, and neutrals are very high and, over threshold energies, they presumably collide to yield new species [Eqs. (1)–(4)] which will be expected to appear as sidebands in ion distribution one charge up or down. If one chooses a given precursor ion distribution, say that for Fe^{2+}, the corresponding recombined ions will be observed as a sideband in the ion distribution for one charge lower, namely, Fe^+. Similarly, ionized ions will be observed in ion

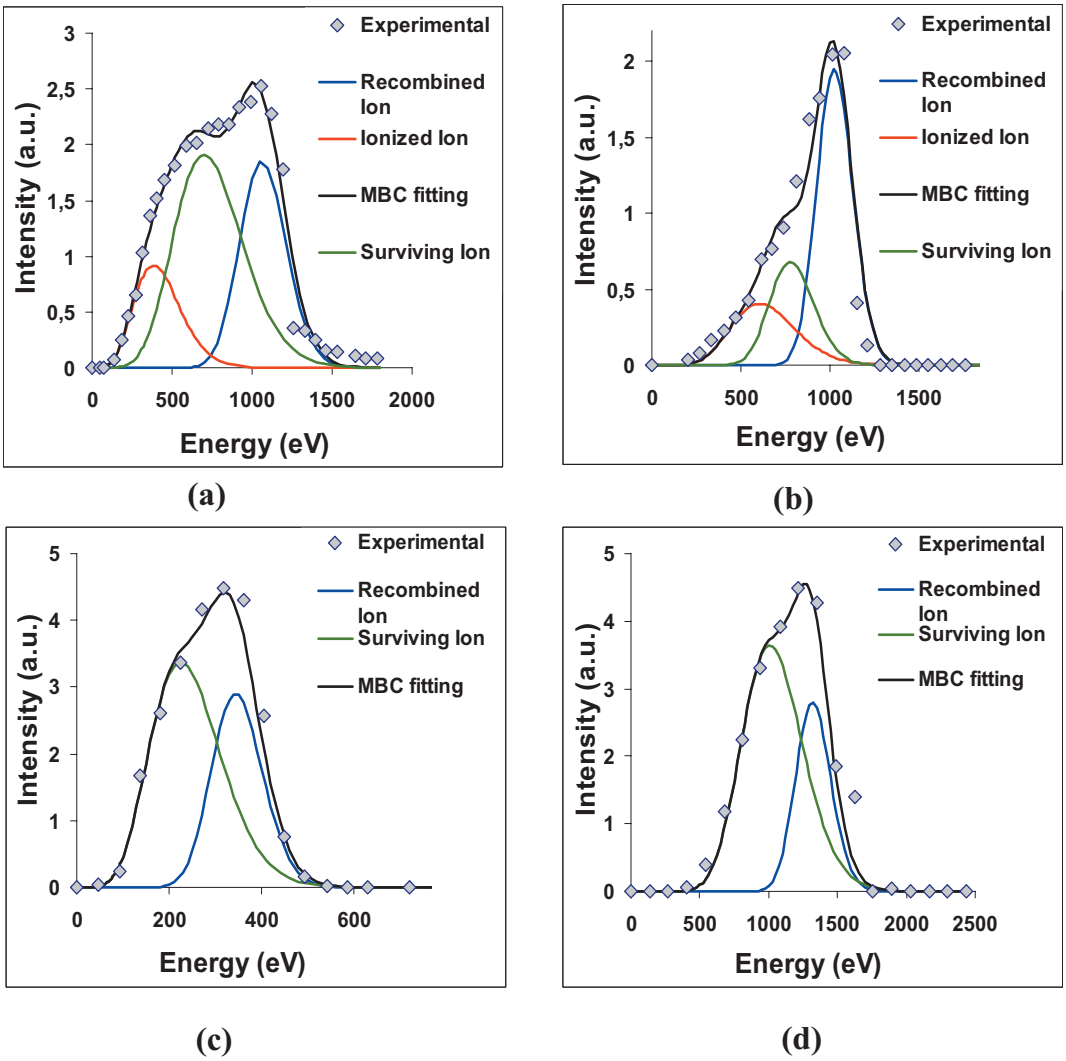

FIG. 3. (Color) Assorted examples of fittings to the experimental distributions for Fe and Ni ions at various laser fluences: (a) Ni^{2+} at 14.7 J cm^{-2}; (b) Ni^{3+} at 6.0 J cm^{-2}; (c) Fe^{2+} at 5.6 J cm^{-2}; (d) Fe^{3+} at 9.2 J cm^{-2}. The so-called surviving "precursor" ion of a distribution is the ion observed without change of charge.

distributions one charge higher, in this case, Fe^{3+}. These contributions are thus markers of fundamental ablation processes as band areas proportional to the density of the ions created.

For medium- and high-energy laser fluences, the expected distribution is a sum of the surviving "precursor" and the ionic and recombination contributions:

$$F(v_x,v_c) = \sum_{i=1}^{3} \lambda_i A(m/2\pi kT)^{3/2} v_x^3 \exp[-m(v_x - v_k - v_c)^2/2kT] \tag{6}$$

where v_{ci} is the Coulomb velocity of the ionized precursor or recombined ions observed at the surviving "precursor" charge and λ_i its relative contribution. The ion that underwent recombination initially had one charge higher than the surviving precursor and is ejected with a higher Coulomb velocity, appearing as a sideband or shoulder at higher energy. On the other hand, the ion that later underwent ionization initially had a charge lower than the group in which it is observed, its Coulomb velocity is smaller, and appears as a sideband at lower energy. The model is further supported by the weak sensitivity of the ion velocities to the target-skimmer distance (experimental: 5 to 13 cm) [18]. Thus the resultant MBC ion distribution is created by electron-neutral or electron-ion collisions before ejection into the plume. No effects due to double ionization have been observed for the fluences investigated. It should be stressed that VDs for sideband velocities of ions can only be compared with main band features (of the surviving "precursor") if the experimental conditions are identical. Indeed this is the case for ablation carried out at a fluence of choice. Velocity distributions at different fluences are not comparable and the mechanisms and processes in the different ablation plumes vary.

Examples of experimental distributions for Fe^{n+} and Ni^{n+}, fitted to linear combinations of single MBC distributions, are shown in Fig. 3. Calculating v_k as the sonic velocity [16,17], $(\gamma kT/m)^{1/2}$, and fitting the distribution to Eq. (6) yields the Coulomb and total averaged velocities. These are shown in Table I in units of 10^4 m s^{-1} for fluences in the range

TABLE I. Comparison of the Coulomb and average total velocities (in 10^4 m s^{-1}, from MBC distributions) characteristic of the Fe and Ni ions ejected from pulsed laser ablation at a number of fluences. The source (ions, neutral) to the distributions for an observed ion are indicated underlined on the top of the table (e.g., for the observed Fe^+ the source ions are Fe^+ and Fe^{2+}).

Source ion		Fe^+		Fe^{2+}		Fe^{3+}		Fe^{4+}	
Fluence ($J\ cm^{-2}$)	**Observed ion**	v_c	v_t	v_c	v_t	v_c	v_t	v_c	v_t
13.1	Fe^+	0.53	1.86	3.41	4.26				
	Fe^{2+}			3.29	4.43	5.39	5.87		
	Fe^{3+}					5.29	6.15	6.85	7.25
	Fe^{4+}							6.74	7.48
9.2	Fe^+	0.52	1.86	2.71	3.71				
	Fe^{2+}			2.70	3.78	4.84	5.62		
	Fe^{3+}					4.83	5.68	6.26	6.70
	Fe^{4+}							6.13	6.70
6.8	Fe^+	0.53	1.61	2.49	3.69				
	Fe^{2+}			2.64	3.71	4.70	5.49		
	Fe^{3+}					4.78	5.57	6.14	6.57
	Fe^{4+}							6.12	6.57

Source ion		Ni^0		Ni^+		Ni^{2+}		Ni^{3+}		Ni^{4+}	
Fluence ($J\ cm^{-2}$)	**Observed ion**	v_c	v_t	v_c	v_t	v_c	v_t	v_c	v_t	v_c	v_t
14.7	Ni^+	0.67	1.58	2.11	3.16	3.74	4.38				
	Ni^{2+}			2.25	3.16	3.74	4.47	5.33	5.86		
	Ni^{3+}					3.98	4.51	4.89	5.80	6.23	6.66
	Ni^{4+}							5.39	5.63	6.07	6.71
10.5	Ni^+	0.32	1.15	2.11	3.16	3.74	4.38				
	Ni^{2+}			2.25	2.97	3.29	4.20	4.77	5.21		
	Ni^{3+}					3.62	4.20	4.69	5.24	5.52	5.89
	Ni^{4+}							4.65	5.23	5.52	5.89
6.8	Ni^+	--	--	2.05	2.97	3.38	4.20				
	Ni^{2+}			1.92	2.97	3.29	4.20	4.63	5.0		
	Ni^{3+}					3.30	4.18	4.63	5.0	4.43	5.80
	Ni^{4+}							4.66	5.03	4.46	5.83

6.8–14.7 J cm^{-2}. The distributions have two or three components as underlined in the heading of Table I for each observed ion shown in the column. VDs for ablated Fe ions have only one sideband, in contrast with those of Ni ions that have two. The good matching of the recombined Fe ion velocities and those of the surviving precursor with one charge higher may be stressed. Ni ion VDs have two sidebands corresponding to the recombined and the ionized ions that match the velocities of the ion one charge lower than that of the surviving precursor ion and that one charge higher, respectively. For a given fluence, the agreement for both the Coulomb and total velocities is surprisingly good and thus indicates that collisions, recombinations, and ionizations take place before ion ejection. In addition, the overall process

TABLE II. Ablation branching ratios for the recombination processes in Fe ions. $[Fe^{n+}]^{q+}$ stands for an observed Fe^{q+} ion originated as Fe^{n+}.

Fluence (J cm^{-2})	Computed $\frac{[Fe^{2+}]^+}{[Fe^{2+}]^+ + [Fe^{2+}]^+}$	Computed $\frac{[Fe^{3+}]^{2+}}{[Fe^{3+}]^{2+} + [Fe^{2+}]^{2+}}$	Computed $\frac{[Fe^{4+}]^{3+}}{[Fe^{4+}]^{3+} + [Fe^{3+}]^{3+}}$
13.1	20%	18%	27%
9.2	27%	37%	47%
6.8	37%	47%	51%
5.6	10%	75%	⋯
2.6	17%	88%	⋯

takes place on a time scale much shorter than the laser duration and has been estimated to be the time required for an ion to pass the plasma thickness in the picosecond range (see below).

The ionization and recombination branching ratios for ion-electron collisions may be calculated from the integrated velocity distributions. These are listed in Table II for Fe ions. It may thus be concluded that, within the initial plasma, the ionization rates for Fe ions [19] are at least three orders of magnitude smaller than those for recombination. Significant contributions by ionization processes to the total distribution are observed for Ni ions from a Ni_2MnGa target (and indeed from any other Ni containing alloy including Ni metal).

While the proportionality between the Coulomb energy and the ion charge has been assumed [12,20], once the distributions have been confirmed as following MBC distributions, analysis of this relationship may be considered further. Figure 4 depicts a plot of the measured squared Coulomb velocity v_c^2 of the Fe and Ni ions versus the ion charge from a NiFe target. The experimental data fit a second order polynomial well. Assuming initially that the best fit is a straight line with an intercept at the origin, indicating no charge and hence no Coulomb velocity, all the ions would then leave the plasma with a Coulomb velocity v_c balanced by an electric field E_{eff} $(1/2mv_c^2 = ZeV_{\text{eff}})$ independent of other contributions to the total velocity. Although the laser radiation penetration into the metal follows an exponential law, it may be assumed for qualitative purposes to be characterized by an equivalent average penetration depth. For the metals and alloys studied at $\lambda = 532$ nm, the commonly accepted penetration depth is ≈ 20 nm. For a charged species ejected with Coulomb velocities of the order of 2.2×10^4 m s^{-1}, the electric field perpendicular to the solid is $E_{\text{eff}} = 14.5 \times 10^6$ V m^{-1} and the electron or positive charge density needed to create the required field [20] $(E_{\text{eff}} = 1.8 \times 10^{-6}\ \Delta nx)$ is $\Delta n \approx 3.9 \times 10^{19}$ electron cm^{-3}. Hence, a substantial number of photoelectrons have to be ejected from the skin of the ablated metal before the ions are driven out, a fundamental conclusion apparently not considered hitherto. In addition, the constant slope of the energy–ion-charge relationship implies the presence of an average high field experienced by the charged ions in the duration of the ablation pulse. An increase of energy over the straight line (Fig. 4) would imply a further increase of the field for the higher

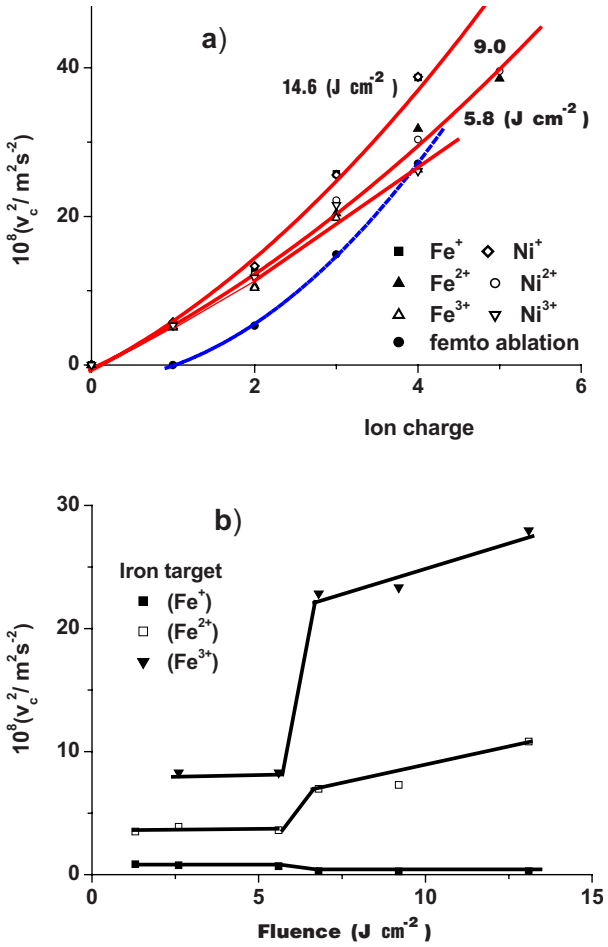

FIG. 4. (Color online) Plots of the squared Coulomb velocity (or energy and/or mass) for (a) Fe and Ni ions from an NiFe alloy target at 14.6, 9.0, and 5.8 J cm^{-2} nanosecond laser fluences and 3.8 and 3.2 J cm^{-2} femtosecond laser fluences and (b) Fe and Ni ions from FeNi alloy targets, respectively (fluence 6 J cm^{-2}). Solid curves in (a) are polynomial fittings to experimental points.

charges created later in the multiphoton absorption process. In view of the foregoing, it is seen that neither the ablation plume nor the surface radiation-metal plasma are (quasi) neutral during the nanosecond ablation process.

For the ablation measurements with NiFe, the quadratic term of the fluence–Coulomb-energy best fit is positive. Hence, once the electric field is shaped to drive out the electrons, a higher field is generated on the ns time scale. Figure 4(a) shows this type of behavior for nanosecond laser fluences of 14.6, 9.6, and 5.8 J cm^{-2}, respectively. Furthermore, these results demonstrate the conservation of energy of the ejected ions from the same zone and field together with the accuracy in the velocity distributions. The ratio of the squared Coulomb velocity (v_c^2) for Fe and Ni ions used in the plot is 1.045, very close to the ratio of their inverse masses, and hence the Fe and Ni ions are expelled with the same kinetic energy as expected if the driving force results from an electric field. The correlation coefficients of the second-degree polynomial fittings are 0.995, 0.992, and 0.9994.

The approximation of neglecting relaxation of the electrostatic field into the metal bulk is sensible for near fluence

threshold ablation since the time to build up the electrical field is close to that of the pulse width and hence the electron averaged drift velocity is small. Simple calculations with such a model indicate that the time to cross the surface depth is of the order of 1 ps. At higher fluence there is a balance between the photoelectrons pumped by the pulsed laser to yield the electrostatic field and its spread by the electron drift velocity. Experiments in the picosecond region are clearly required to characterize the relaxation time ($ns > \tau > 1$ ps) to simulate the ablation process in metals.

The electric field intensities within the ejection zone experienced by the ions may also be used as a marker to probe processes that change with fluence. In the study on the Fe target, noticeable changes in v_c^2 appear near 6 J cm^{-2}, namely, a small decrease for Fe^+, a significant increase for Fe^{2+}, and a still larger increase for Fe^{3+} [Fig. 4(b)]. These effects presumably arise from the soft matter structure of the skin plasma and the building up of the electrical field. Comparable experiments with a pure Ni target yield a transition near threshold (2.3 J cm^{-2}) followed by a smooth increase in the series $Ni^+ < Ni^{2+} < Ni^{3+}$. Measurements with a NiFe target indicate a jump at low fluence in close similarity to Ni, but, in contrast with Fe, suggesting that in Ni the creation of the electric field is more rapid.

Differences in velocity distributions of Fe ions using femtosecond (fs) lasers (35 fs pulses, 10 Hz, 0.8 μJ at 800 nm, up to 4 J cm^{-2}) and nanosecond pulsed laser provide time scales for some ablation processes that are involved. Femtosecond lasers yield only single MBC distributions with no recombinations or ionizations at fluences up to 4 J cm^{-2}, not shown here. These processes thus require $<10^{-9}$ s for completion and hence reaction rate constants within the original plasma of $k > 10^{-7}$ cm^3 molecule^{-1} s^{-1}, roughly in accord with estimated collision numbers. In fs ablation, the Coulomb ejection velocity for singly ionized ions (M^+) is negligible compared with that from nanosecond ablation [Fig. 4(a)], with a significant increase for more highly charged ions. Consequently, electrons from the plasma are ejected after the formation of the M^+ ion, generating the positive electrostatic field before M^{2+} and more highly charged ions are created. The ionization processes are thus sequential and completed for the M^+ ion in <35 fs, the time also required for photoelectron ejection. Further, the energies of the ejected ions (Ni^+ and Fe^+, etc.) from NiFe and Ni_2MnGa alloys are equal within experimental error and provide a good example of energy conservation. These time scales are crucial for distinguishing between photothermal and photophysical effects, long observed in ablation [2].

IV. CONCLUSIONS

It has been shown that ablation with lasers in the nanosecond region at medium and high fluences on metal and alloys proceeds via electron-ion recombination and/or ionization processes. These phenomena are not observed in the femtosecond regime. The contributions of recombinations and ionization processes to the observed ion distributions depend on the laser pulse width. This, in turn, may be used for determining the rates of ion-electron collisions in plasmas, a possibly unique experimental method for characterizing such rate processes under these conditions. In addition, the branching ratios yield comparative measurements of recombination and ionization rates under plasma conditions. Knowledge of one permits calculation of the other.

It has been demonstrated that the ejection of ions at high velocity is only feasible if these are driven out by an electrostatic field created on the skin of the metal resulting from the ejection of photoelectrons produced by laser absorption. The electric field is of sufficient duration to yield an averaged acceleration of each charged ion. Ion-electron collisions and the creation of an electric field, coupled with a variety of relaxation processes, are necessary components for constructing a realistic model for laser ablation on metals.

The interaction of high-density radiation with matter and further mass detection of ions may be applied as an extension of LIBS for the analysis of metals and alloys and also for sensitive structural characterization. The advantages of mass detection over light emission as an analytical tool for studying the composition of metals have clearly been demonstrated.

ACKNOWLEDGMENTS

We thank Dr. D. Husain (Cambridge, UK) for helpful discussions. This work was supported by MEC (Madrid, Spain), Consolider (MEC), GV/EJ (Vitoria), and UPV/EHU.

[1] T. D. Bauerle, *Laser Processing and Chemistry* (Springer, Berlin, 2000).
[2] W. W. Dudley, *UV Laser: Effects and Applications in Material Sciences* (Cambridge University Press, Cambridge, 1996).
[3] L. J. Rodienski, Spectrochim. Acta, Part B **57**, 1104 (2002).
[4] P. Yaroshchyk, D. Body, R. J. S. Morrison, and B. L. Chadwick, Rev. Sci. Instrum. **75**, 5050 (2004).
[5] D. A. Rusak, B. C. Castle, B. W. Smith, and J. D. Winefordner, Crit. Rev. Anal. Chem. **27**, 257 (1997).
[6] K. Song, Y.-I. Lee, and J. Sneddon, Appl. Spectrosc. Rev. **32**, 183 (1997); E. Tognoni, V. Palleschi, M. Corsi, and G. Cristoforetti, Spectrochim. Acta, Part B **57**, 1115 (2002).
[7] L. Laska *et al.*, Czech. J. Phys. **54**, 370 (2004), Part 1-3, Suppl. C.
[8] L. Torrisi and D. Margarone, Plasma Sources Sci. Technol. **15**, 635 (2006), and references therein.
[9] J. R. Goldman and J. A. Prybyla, Phys. Rev. Lett. **72**, 1364 (1994). Note that electron-ion collisions were not regarded as a feasible energy relaxation mechanism.
[10] L. Torrisi, F. Caridi, A. Picciotto, M. Margarone, and A. Borrielli, J. Appl. Phys. **100**, 093306 (2006).
[11] L. Torrisi, F. Caridi, A. Picciotto, and A. Borrielli, Nucl. Instrum. Methods Phys. Res. B **252**, 183 (2006).
[12] L. Torrisi, S. Gammino, L. Andò, and L. Laska, J. Appl. Phys.

91, 4685 (2002).
[13] S. Amoruso, M. Armenante, V. Berardi, R. Bruzzese, G. Pica, and R. Velotta, Appl. Surf. Sci. **106**, 507 (1996).
[14] S. Amoruso, V. Berardi, R. Bruzzese, N. Spinelli, and X. Wang, Appl. Surf. Sci. **129**, 953 (1998).
[15] *Handbook of Chemistry and Physics*, edited by D. R. Lide, 87th ed. (CRC Press, Boca Raton, FL, 2006).
[16] R. Kelly, J. Chem. Phys. **92**, 5047 (1990).
[17] A. Peterlongo, A. Miotello, and R. Kelly, Phys. Rev. E **50**, 4716 (1994).
[18] Experiments with a gas background pressure and detection of the total density of ions cause significant distribution dependence with the target-detector distance. Cf. N. M. Bulgakova and A. V. Bulgakov, Phys. Rev. E **62**, 5624 (2000); O. A. Novodvorsky, O. D. Khramova, C. Wenzel, J. W. Bartha, and E. O. Filippova, J. Appl. Phys. **94**, 3612 (2003).
[19] S. N. Vahar, M. A. Bautista, and A. K. Pradham, Astrophys. J. **479**, 497 (1997).
[20] A. Frank-Kamenetski, *Plasma, the Fourth State of Matter*, Spanish translation (MIR, Moscow, 1970).